Atmospheric
Chemistry
and Physics
Discussions

Open Access

EGU

1   **Background aerosol over the Himalayas and Tibetan Plateau:**

2   **observed characteristics of aerosol mass loading**

3

4   Bin Liu[1], Zhiyuan Cong[1,4], Yuesi Wang[2], Jinyuan Xin[2], Xin Wan[1], Yuepeng Pan[2],

5   Zirui Liu[2], Yonghong Wang[2], Guoshuai Zhang[1], Zhongyan Wang[1], Yongjie Wang[1]

6   Shichang Kang[3,4*]

7

8   1 Key Laboratory of Tibetan Environment Changes and Land Surface Processes, Institute of Tibetan Plateau

9   Research, Chinese Academy of Sciences (CAS), Beijing 100101, China

10

11   2 State Key Laboratory of Atmospheric Boundary Layer Physics and Atmospheric Chemistry (LAPC), Institute of

12   Atmospheric Physics, CAS, Beijing 100029, China

13

14   3 State Key Laboratory of Cryospheric Sciences, Cold and Arid Regions Environmental and Engineering Research

15   Institute, CAS, Lanzhou 730000, China

16

17   4 CAS Center for Excellence in Tibetan Plateau Earth Sciences, Chinese Academy of Sciences, Beijing 100101,

18   China

19

20   **Correspondence to:**

21   Shichang Kang

22   Tel: +86-0931-4967368; shichang.kang@lzb.ac.cn

23

Atmospheric
Chemistry
and Physics

Open Access

EGU

Discussions

24 **Abstract**

25   To investigate the atmospheric aerosols of the Himalayas and Tibetan Plateau (HTP), an

26   observation network was established within the region's various ecosystems, including at the

27   Ngari, Qomolangma (QOMS), Nam Co, and Southeastern Tibetan (SET) stations. In this

28   paper we illustrate aerosol mass loadings by integrating *in situ* measurements with satellite

29   and ground-based remote sensing datasets for the 2011-2013 period, on both local and large

30   scales. Mass concentrations of these surface atmospheric aerosols were relatively low and

31   varied with land cover, showing a general tendency of Ngari and QOMS (barren sites) > Nam

32   Co (grassland site) > SET (forest site). Daily averages of online $PM_{2.5}$ (particulates with

33   aerodynamic diameters below 2.5 μm) at these sites were sequentially 18.2 ± 8.9, 14.5 ± 7.4,

34   11.9 ± 4.9 and 11.7 ± 4.7 μg m^{-3}. Correspondingly, the ratios of $PM_{2.5}$ to total suspended

35   particles (TSP) were $27.4 \pm 6.65\%$, $22.3 \pm 10.9\%$, $37.3 \pm 11.1\%$ and $54.4 \pm 6.72\%$. Bimodal mass

36   distributions of size-segregated particles were found at all sites, with a relatively small peak in

37   accumulation mode and a more notable peak in coarse mode. Diurnal variations in fine

38   aerosol masses generally displayed a bi-peak pattern at the QOMS, Nam Co and SET stations

39   and a single-peak pattern at the Ngari station, controlled by the effects of local

40   geomorphology, mountain-valley breeze circulation and aerosol emissions. Mineral content in

41    $PM_{2.1}$ samples gave fractions of 26% at the Ngari station and 29% at the QOMS station, or

42   ~2-3 times that of reported results at human-influenced sites. Furthermore, observed evidence

43   confirmed the existence of the aerodynamic conditions necessary for the uplift of fine

44   particles from a barren land surface. Combining surface aerosol data and atmospheric-column

45   aerosol optical properties, the TSP mass and aerosol optical depth (AOD) of the Multi-angle

Atmospheric
Chemistry
and Physics

Open Access

EGU

Discussions

46   Imaging Spectroradiometer (MISR) generally decreased as land cover changed from barren to

47   forest, in inverse relation to the $PM_{2.5}$ ratios. The seasonality of aerosol mass parameters was

48   land-cover dependent. Over forest and grassland areas, TSP mass, $PM_{2.5}$ mass, MISR-AOD

49   and fine-mode AOD were higher in spring and summer, followed by relatively lower values

50   in autumn and winter. At the barren site (the QOMS station), there were inconsistent seasonal

51   variations between surface TSP mass ($PM_{2.5}$ mass) and atmospheric column AOD (fine-mode

52   AOD). Our findings implicate that, HTP aerosol masses (especially their regional

53   characteristics and fine particle emissions) need to be treated sensitively in relation to any

54   assessments of their climatic effect and potential role as cloud condensation nuclei and ice

55   nuclei.

56

57

58

59

60

61

62

63

64

65

66

67

Atmospheric
Chemistry
and Physics
Discussions

Open Access

EGU

1 Introduction

68

69   Atmospheric aerosols undergo changes in their microphysical, chemical and optical

70   properties, especially in high-altitude mountain regions. These changes primarily determine

71   their roles in modifying regional climate, cryosphere and hydrology. This is particularly true

72   for the Himalayas and Tibetan Plateau (HTP) region, which is surrounded by Asian dust and

73   strong anthropogenic emissions. These natural and human-originated airborne chemicals,

74   such as light-absorbing materials, reactive nitrogen and heavy metals can exert impacts on

75   regional monsoon rainfall (e.g., Ramanathan et al., 2005; Lau et al., 2006), snow/ice albedo

76   (e.g. Ming et al., 2008; Xu et al., 2009; Qu et al., 2014), nitrogen deposition (Liu et al., 2013;

77   Liu et al., 2015) and meltwater composition (e.g., Zhang et al., 2014). Although these effects

78   remain poorly understood, it is of first-order importance to characterize these remote

79   atmospheric aerosols.

80   In the HTP, aerosol optical properties and chemical compositions have been observed

81   almost entirely at a few specific sites. Ground-based measurements have focused on the

82   relatively small concentrations of fine particles and total suspended particle (TSP) in the

83   HTP's atmospheric surface layer (Zhao et al., 2013; Xu et al., 2014). Satellite and

84   ground-based remote sensing have also been employed and have pointed to a low aerosol

85   optical depth (AOD) in this region (Xia et al., 2008; Xia et al., 2011; Yan et al., 2015).

86   Mineral dust has been identified as one of the main aerosol components in the central

87   Himalayas (Decesari et al., 2010) and the central TP (Zhang et al., 2001; Cong et al., 2007;

88   Kang et al., 2016). Analysis of dust plumes from the surrounding deserts (the Taklimakan,

89   Gobi and Southwest Asian deserts) and itself has indicated some potential source areas of

Atmospheric
Chemistry
and Physics
Discussions

Open Access

90   atmospheric particulates (Huang et al., 2007; Liu et al., 2008; Xia et al., 2008). However,

91   these results have revealed only the somewhat pristine characteristics of HTP aerosols,

92   dependent largely upon a significant understanding of mineral dust. Much uncertainty

93   remains over the correct evaluation of aerosol sources, transportation and deposition,

94   especially in relation to a much wider variety of aerosol species. Furthermore, the mountains

95   produce   extensive   mountain-valley   breezes,   and   alpine   glacier/snow   and

96   stratosphere-troposphere exchanges. These conditions could in turn affect aerosol properties

97   via transportation and chemical processes by facilitating the upward diffusion of aerosol

98   matters (Decesari et al., 2010; Cong et al., 2015) and by changing the oxidizing capacity of

99   the troposphere (Lin et al., 2008). Hence there are additional obstacles in understanding HTP

100   atmospheric aerosols.

101   Anthropogenic emissions into this region occur occasionally and are dependent on

102   local/regional atmospheric dynamics. During the pre-monsoon period, "Atmospheric Brown

103   Cloud" stacks up in the southern foothills of the Himalayas (Ramanathan et al., 2001).

104   Mountain-valley breeze circulations allow these aerosols to spread upslope and then can

105   enhance the concentrations of carbonaceous and inorganic matters in fine aerosols over the

106   Himalayas (Decesari et al., 2010; Babu et al., 2011; Cong et al., 2015; Lüthi et al., 2015).

107   Additionally, the South Asian summer monsoon system is one of the important atmospheric

108   dynamics in the transportation of pollutants to the HTP region from southern and southeastern

109   Asia (Liu et al., 2013; Sheng et al., 2013). Consequently, light-absorbing substances (such as

110   black carbon) have received special attention. Studies have raised the hypothesis that a

111   suppression of the Southern Asian monsoon through a weakening of the meridional surface

Atmospheric
Chemistry
and Physics
Discussions

Open Access

EGU

112   temperature gradient (Ramanathan et al., 2005), is likely to enhance regional monsoonal

113   rainfall in northern India, the Himalayas, and the southern Tibetan Plateau (TP) through the

114   "elevated-heat-pump" effect (Lau et al., 2006). Further, the post-depositional effect of

115   decreasing snow/ice albedo is likely to lead to reductions in the HTP glaciers (Ming et al.,

116   2008; Xu et al., 2009; Qu et al., 2014). However, the validity of the above hypothesis strongly

117   depends on the characteristics and spatial-temporal variations in these particles (principally in

118   mass loadings, chemical compositions, size distributions and optical properties), and their

119   related atmospheric processes.

120   In general, the HTP, as a unique upland region where the relatively pristine tropospheric

121   environment is juxtaposed with Asian anthropogenic emissions, is highly suitable for the

122   study of background atmospheric aerosols and the interactions between natural and

123   anthropogenic emissions, processes which may have far-reaching environmental and climatic

124   consequences (Lawrence, 2011; Vernier et al., 2011).

125   It is imperative, therefore, that the first comprehensive observation of HTP atmospheric

126   background aerosols be conducted during the 2011-2013 period, basing on four stations

127   located in different ecosystems. Accordingly, we present in this study online $PM_{2.5}$ (particles

128   with aerodynamic diameters ≤ 2.5 μm) concentrations and filter-sampled particles, as well as

129   the size distributions of these size-segregated particles (Section 3.1). The diurnal variations in

130   fine aerosol masses are also discussed with particular reference to local geomorphology,

131   source emissions and meteorological settings (Section 3.2). As part of our research, we

132   attempted to integrate these *in situ* observations with aerosol optical properties derived from

133   both ground-based and satellite remote sensing, aiming to construct a topographical view of

Atmospheric
Chemistry
and Physics
Discussions

134   their spatial and seasonal patterns (Section 3.3).

2 Materials and Methods

2.1 Monitoring sites and the regional environment

137   The HTP is the greatest upland region of the Eurasian continent in the Northern

138   Hemisphere's middle-low latitudes, and composes landscapes covered mainly by alpine forest,

139   grassland/meadow, barren areas and patchy glacier/snow cover. We take 'upland' in the HTP

140   region to be land above 2800 m asl; if so, this region has an upland area of ~5,000,000 km^2

141   (Fig. 1a). Four comprehensive observation platforms were established within different

142   landscapes, including the Ngari station (79°42′E, 33°23′N, 4,264 m asl), the

143   Qomolangma/Everest (QOMS) station (86°57′E, 28°21′N, 4,300 m asl), the Nam Co station

144   (90°57′E, 30°46′N, 4,746 m asl), and the SouthEastern Tibet (SET) station (94°44′E, 29°46′N,

145   3,326 m asl) (Figs. 1 and S1). The high-altitude, inland topography produces a generally cold,

146   arid and windy climate across most of the HTP. Additionally, the atmospheric circulation

147   systems (including the South Asian Monsoon, the East Asian Monsoon, and the Westerlies)

148   control the seasonal and spatial variations in precipitation patterns, i.e., winter-spring

149   precipitation in the western HTP (Pamir areas), monsoonal rainfall in the southeastern and

150   eastern TP and Himalayas, and sparse precipitation in the northern regions (Fig. S2).

151   Records of daily air pressure (P), temperature (T), relative humidity (RH), precipitation

152   amount (PA), horizontal wind speed (WS) and wind direction (WD) observed at these stations

153   displayed regional variability and seasonality of meteorology in the HTP during 2011-2013

154   (Fig. 2). Generally, the levels of P were clearly different, and decreased with ascending

Atmospheric
Chemistry
and Physics
Discussions

155   altitude, showing values of 605.4±3.7 hPa at the Ngari station, 604.6±3.2 hPa at the QOMS

156   station, 570.7±4.4 hPa at the Nam Co station and 679.5±2.9 hPa at the SET station (±1.0

157   standard error). The altitude effect may have also influenced the horizontal WS values, which

158   were 2.7±1.1, 4.3±1.6, 3.4±1.4 and 1.1±0.7 m s^{-1} for the Ngari, QOMS, Nam Co, SET

159   stations, respectively. The PA was controlled by Asian monsoon systems within annual

160   ranges of 173.3-243.8 mm, 444.2-488.2 mm and 436.6-905.8 mm at the QOMS, Nam Co and

161   SET stations, respectively. The lowest annual PA (40.9-125.3 mm) and mean RH

162   (29.2±14.7%) were observed at the Ngari station. The greater seasonal variability in T noted

163   at the Ngari station compared to other stations, i.e., from the lowest value (-10.6±4.8 ℃) in

164   December-February to the highest value (14.0±3.1 ℃) in June-August, can be explained by its

165   position far inland and its attendant climate.

166   **2.2 Observation protocols for HTP atmospheric aerosols**

167   Detailed information of HTP aerosol measurements are presented in Table 1, and include

168   the physical, chemical and optical properties of atmospheric aerosols at the Ngari, QOMS,

169   Nam Co and SET stations.

170   RP 1400 series tapered element oscillating microbalance (TEOM) machines were installed

171   and operated at each station to collect PM$_{2.5}$ data from the autumn on 2011 onwards. PM$_{2.5}$

172   mass was weighed and quantified based on the oscillation frequency of the tapered tube

173   (Patashnick and Rupprecht, 1991). Their values were recorded at 5-min intervals. Values

174   ranged from 0-5 g m^{-3}, with a resolution of 0.1 μg m^{-3} and a precision of ±0.5 μg m^{-3} over a

175   24-hour average (Xin et al., 2015). At each station, size-segregated airborne particles (with

Atmospheric
Chemistry
and Physics
Discussions

176   the diameters of <0.43 μm, 0.43-0.65 μm, 0.65-1.1 μm, 1.1-2.1 μm, 2.1-3.3 μm, 3.3-4.7 μm,

177   4.7-5.8 μm, 5.8-9.0 μm, and >9.0 μm, respectively) were collected weekly using airborne

178   particle nine-stage samplers (Andersen Series 20-800, USA) at a flow rate of 28.3/l min^{-1}.

179   Quartz filters and cellulose membranes (with diameters of 81 mm) were applied alternately

180   for measuring different chemical species, with a collection time of 72 h per week (always

181   over the Monday-Wednesday period). Before and after sampling, the filters were weighed

182   using a microbalance (sensitivity ±0.01 mg) after drying for 48 h, at 25 ℃ and 50% humidity

183   (Xin et al., 2015). Mass concentrations of these filtered samples were in turn obtained

184   according to the standard sampling volume.

185   2.3 Methods of data analysis

186   The baseline properties of atmospheric aerosol mass revealed a relatively stable and low

187   aerosol loading, excluding the possible perturbations (Kaufman et al., 2001; Xia et al., 2011).

188   Following Kaufman et al. (2001), we calculated the median of 50 consecutive hour-average

189   values of online $PM_{2.5}$ masses over 2-3 day, and removed data sequences with standard

190   deviations higher than those of the whole time series by repeatedly shifting the running

191   medians by one measurement point. The standard deviation thresholds were 24 μg m^{-3} at the

192   Ngari station, 13 μg m^{-3} at the QOMS station, 9 μg m^{-3} at the Nam Co station, 11.7 μg m^{-3} at

193   the SET station. Consequently, the any remaining datasets were considered the time series of

194   baseline $PM_{2.5}$ masses.

195   We applied monthly Level 3 datasets of Multi-angle Imaging Spectroradiometer (MISR) to

196   characterize atmospheric column AOD (at 550 nm) over the HTP for 2011-2013. Level 2.0

Atmospheric
Chemistry
and Physics
Discussions

Open Access

EGU

197   Aerosol Robotic Network (AERONET) datasets that at the QOMS station, and Level 1.5

198   datasets at the Nam Co station were also used to address fine-mode AOD (at 500 nm).

199   Additionally, a global 0.5 km land cover climatology that derived from Moderate Resolution

200   Imaging Spectrometer (MODIS) (Broxton et al., 2014) was converted to a 1×1 degree pixel

201   resolution using ArcGIS software, which provided the HTP's land cover datasets.

202   **3 Results and discussion**

203   **3.1 Mass concentrations of online $PM_{2.5}$ and segregated particles**

204   Figure 3 and Table 2 show the time series and statistics for online $PM_{2.5}$ measurements

205   monitored at four HTP stations during 2011-2013. The daily mean concentrations were

206   18.2 ± 8.9 µg m^{-3} at the Ngari station, 14.5 ± 7.4 µg m^{-3} at the QOMS station, 11.9 ± 4.9 µg m^{-3} at

207   the Nam Co station, and 11.7 ± 4.7 µg m^{-3} at the SET station. Fine aerosol masses were

208   therefore generally low but variable against various background atmospheres. These results

209   were comparable with the monitored values of 11.7 ± 15.5 µg m^{-3} at a station in the Qilian

210   Shan Mountains in the northeastern TP (Xu et al., 2014) and 26.6 ± 19.3 µg m^{-3} at a

211   background Himalayan site (Panwar et al., 2013).

212   Baseline levels of hourly $PM_{2.5}$ mass were estimated to be 11.2 ± 3.2 µg m^{-3} at the Ngari

213   station, 9.8 ± 3.1 µg m^{-3} at the QOMS station, 9.8 ± 3.6 µg m^{-3} at the Nam Co station, and

214   9.2 ± 3.0 µg m^{-3} at the SET station (Table 2). The discrepancies between online $PM_{2.5}$ and their

215   baselines were also calculated. Consequently, average percentages and concentration levels

216   were ~22.7% and 4.2 ± 14.0 µg m^{-3} at the Ngari station, ~16.6% and 2.1 ± 2.0 µg m^{-3} at the

217   QOMS station, ~6.8% and 0.8 ± 5.3 µg m^{-3} at the Nam Co station, and ~10.3% and 1.2 ± 6.6 µg

Atmospheric
Chemistry
and Physics
Discussions

Open Access

EGU

218   m^{-3} at the SET station (Table 2). Relatively great distinctions therefor were found at the Ngari

219   and QOMS stations. Significant variations, indicated by their daily frequency curves, also

220   occurred at the Ngari and QOMS stations, and were associated with episodes of high

221   concentration events (Fig. 4). These results implied a disturbance in the high-concentration

222   aerosol masses of inland Asia associated with possible dust impact, and dependent upon

223   proximity to local arid and barren areas(for their typical landscapes, see Fig. S1).

224   We further assessed mineral matter content in fine particles by analyzing elements and

225   water-soluble inorganic ions in $PM_{2.1}$ samples with inductively coupled plasma mass

226   spectroscopy (ICP-MS) and ion chromatography (IC). Mineral dust content was assumed to

227   be a mixture of mainly crustal oxides, i.e. SiO_2, Al_2O_3, CaO, Fe_2O_3, K_2O, Na_2O and MgO. A

228   detailed description of this approach can be found in Xin et al. (2015). Mineral content was

229   about 26% at the Ngari station and 29% at the QOMS station. Our measurements revealed the

230   impact of regional dust emissions, even for fine particles, over the HTP's barren areas.

231   Proportions were 2-3 times those of $PM_{2.1}$ (mean content 10.8%) measured at a suburban site

232   impacted by heavy air pollutants in North China (Xin et al., 2015), and $PM_{2.0}$ (content of

233     $14 \pm 4\%$) sampled at a human-influenced site in Hungary (Maenhaut et al., 2005).

234   Table 3 shows the statistical results of segregated-particle mass loadings according to

235   weekly filters. These particles exhibited a general tendency of Ngari and QOMS stations

236   (barren sites) > Nam Co station (grassland site) > SET station (forest site) in their mass levels,

237   suggesting a potential effect associated with the HTP land cover. Furthermore, bimodal size

238   distributions of surface-atmospheric particle masses occurred in these upland regions with an

239   average pattern of a relatively small peak in accumulation mode and a more notable peak in

Atmospheric
Chemistry
and Physics
Discussions

240 coarse mode (Fig. 5). This represents an aerosol mass distribution pattern typical of

241 continental background air (Willeke and Whitby, 1975).

3.2 Diurnal variations in mass concentrations of fine aerosols

243   In these background atmospheres, the intensity of diurnal variabilities in $PM_{2.5}$ masses was

244 roughly characterized by their daytime (6:00-18:00 Local Time, LT) to nighttime (18:00-6:00

245 LT) ratios. Their average ratios were ~2.5 at the Ngari station, ~1.1 at the QOMS station, ~0.9

246 at the Nam Co station and ~1.8 at the SET station, based on hourly observations during the

247 2011-2013 period.

248   Higher ratios were found in valleys around the QOMS and SET stations, suggesting a

249 negative impact of mountainous valleys on the diffusion of local aerosol masses. The local

250 geomorphology around these sites is displayed in Figure S3. Conversely, these topographical

251 settings also produced mountain-valley wind circulations aligned with valley orientation, as

252 identified in July and August (Fig. 6). We analyzed the hourly datasets for the summer

253 monsoon period (July and August), as the mid-latitude westerlies are more prevalent during

254 the other periods and thus constrain the influence of synoptic-scale wind. Horizontal WD at

255 the QOMS station was consequently stronger and clearly inverse compared to that at the SET

256 station. Such a topographically-forced circulation can facilitate the spread of aerosols upslope

257 (Decesari et al., 2010; Babu et al., 2011; Cong et al., 2015). This would explain the ratio

258 being lower at the QOM station than at the SET station. The Ngari station is located in a

259 relatively open geomorphological setting, but experiences marked diurnal variations. This

260 phenomenon can be attributed to the dust lift from the barren land surface in the daytime, as

Atmospheric
Chemistry
and Physics
Discussions

Open Access

EGU

261   will be discussed below.

262   The overall patterns of diurnal variability in fine aerosol mass, atmospheric T and RH, as

263   well as in horizontal WD, are shown in Figure 7. These fine particle masses begin to arise

264   during 6:00-8:00 LT, accompanied by an increase in T and a decrease in RH. During the

265   noontime period (10:00-14:00 LT), concentrations decreased again, shown by the trough in

266   their diurnal curves, and coinciding with the highest T and horizontal WD values, and the

267   lowest RH. Consequently, bi-peak patterns in diurnal variations were especially marked for

268   the Nam Co station (whole year), and for the QOM and SET stations (autumn and winter). In

269   contrast, the Ngari station, in the arid Asian interior, evinced a single-peak pattern in diurnal

270   variations. Such variations are typically found in dust provenances (Mbourou et al., 1997;

271   Stout, 2010), resulting from the atmospheric and land surface conditions prevalent during the

272   daytime.

273   In the cases of April 6th-10th 2012, solar radiation (SR) imposed dramatic changes on the

274   soil T and atmospheric T, RH and WS in the morning (Figs. 8 and 9). Here, SR was taken as

275   the downward shortwave radiation and the soil T was the surface soil temperature at 0 cm,

276   measured using an automated weather system at the Ngari station. Increases in atmospheric T

277   and soil T, and a decline in RH, were synchronous from 6:00-7:00 LT, in response to solar

278   heating. SR and soil T values rose increasingly *in tandem* during the 8:30-10:30 LT period,

279   forming a very close relation (R^2=0.96, P=0.98), apparently in response to the arid and barren

280   setting and cloud-free air at that time (Figs. 8 and 9a). Hence, soil T rose from ~ -2.5 ℃ to

281   ~20 ℃ beyond the dew point temperature, and gradually dried out the surface moisture and

282   uppermost layer of land (Fig. 9b). This in turn implied a reduction in the critical dust burst

Atmospheric
Chemistry
and Physics
Discussions

283   threshold for barren conditions (Stout, 2010). Furthermore, the rise in morning WS created an

284   atmospheric dynamic suited to dust suspension in the late morning, when fine materials were

285   transported up from the land surface into the atmosphere (Fig. 8c). The combination of a

286   declining critical dust burst threshold and favorable atmospheric fluctuation induced the

287   increase in fine particles in the atmosphere, with a peak near noontime. During the

288   14:00-18:00 LT period, WS was strongest, with a range of 4-10 m s^{-1}. Dependent upon its

289   intensity, WS can dilute fine particle masses, rather than affect fine particle fluctuations

290   between sandy surfaces and the air. In addition, a decrease in saltation activity prior to the WS

291   dropping has frequently been observed in barren and arid continental interiors, possibly

292   resulting from a reduction in turbulent wind fluctuations in the late afternoon(Stout, 2010).

293   This effect can also restrict dust burst and thus its contribution to ambient fine particle content.

294   These *in situ* observations established that land surface and low-layer atmosphere are the key

295   physical controls of the diurnal $PM_{2.5}$ mass cycle at the Ngari station. They also confirmed

296   that regional dust emissions contributed to the chemical composition of fine aerosols.

297   Bi-peak like diurnal variations in the $PM_{2.5}$ masses at the Nam Co station, located in a

298   grassland site near the great Nam Co Lake (Fig. S3), are shown in Figure 10. The planetary

299   boundary layer height (PBLH) was derived from National Center for Environmental

300   Prediction reanalysis data which used a 1×1 degree pixel and a 3 h temporal resolution

301   (http://www.arl.noaa.gov/gdas1.php). In response to increasing T, the PBLH rose during the

302   daytime from <100 m to >2500 m, associated with a rise in WS (Fig. 10). This combination

303   of factors resulted in a marked diffusion of fine particles, shown by the trough in $PM_{2.5}$

304   concentrations between 10:00 LT and 16:00 LT. This also accounted for the <1 daytime to

Atmospheric
Chemistry
and Physics
Discussions

Open Access

EGU

305   nighttime ratio.

3.3 Spatial and seasonal patterns in atmospheric aerosol masses

307   The monthly mean MISR-AOD values for 2011-2013 suggested HTP atmospheric aerosol

308   masses were generally isolated from surrounding emissions (Fig. 11a). The integrated results

309   of surface-atmospheric aerosol parameters and atmospheric-column aerosol optical properties

310   yielded spatial distributions which suggested that TSP concentrations and MISR-AOD values

311   decreased as land cover varied from barren land, through grassland, to forest (Fig. 11a).

312   The mean fraction of $PM_{2.5}$ to TSP was $27.4\pm6.65\%$, $22.3\pm10.9\%$, $37.3\pm11.1\%$ and

313     $54.4\pm6.72\%$ for the Ngari station, QOMS station, Nam Co station, and SET station,

314   respectively (Fig. 11b). These values increased from barren to forest areas, inversely to TSP

315   masses. A time-average map of the aerosol fine-mode fraction (at 550 nm) for 2011-2013 was

316   also constructed using monthly MODIS Terra (version 5.1) Level 3 values. Its spatial

317   distribution was clearly consistent with the ground-based results recorded at various sites

318   (marked by circles with various colors in Fig. 11b).

319   Figure 12 shows how MISR-AOD values varied along two cross-sections in different

320   months. These results further confirmed a general decline in AOD from northwest to

321   southeast crossing typical plateau landscapes (Section A), and from north to south in the

322   eastern TP (Section B). Furthermore, such a spatial pattern was more notable for

323   April-August, coinciding with the appearance of the Asian tropospheric aerosol layer during

324   this period (Vernier et al., 2011). This may imply the significance of the development of the

325   Asian tropospheric aerosol layer in modulating the AOD level over this plateau.

Atmospheric
Chemistry
and Physics
Discussions

Open Access

EGU

326   TSP mass and MISR-AOD values over HTP forest (SET station) and grassland (Nam Co

327   station) sites shared a common seasonal pattern, with relatively higher values in spring and

328   summer, followed by relatively lower values in autumn and winter (Fig. 13a). At the barren

329   site (QOM station), there were inconsistent seasonal variations between surface-atmospheric

330   TSP ($PM_{2.5}$) and atmospheric column AOD (fine-mode AOD) (Figs. 13a, b). Furthermore,

331   there was no correlation between hourly surface $PM_{2.5}$ mass and fine-mode AOD (at 500 nm)

332   at this site (Fig. S4). Using the Cloud-Aerosol Lidar and Infrared Pathfinder Satellite

333   Observations (CALIPSO), Huang et al. (2007) detected frequent dust plumes in the lower

334   atmosphere (~4-7 km asl) of the western HTP. These dust plumes possibly impacted the

335   vertical distribution of aerosol masses over these barren areas.

336    $PM_{2.5}$ concentrations and fine-mode AOD values were higher in spring and summer than in

337   autumn and winter at HTP forest and grassland sites, but not at the barren site (Fig. 13b).

338   Ratios of $PM_{2.1}$ to TSP were apparently higher at the SET and Nam Co stations compared to

339   QOM station, with a more marked difference in summer and autumn (Fig. 13c). In a

340   background continental atmosphere, fine aerosols mainly originate from biogenic or wildfire

341   emissions. Wild fire was were extremely rare in the HTP region, and fire-related emissions

342   from the Asian Brown Cloud occurred only during the winter and spring, as measured in the

343   Himalayan region (Cong et al., 2015; Decesari et al., 2010). Therefore, biogenic emissions

344   and related products may be essential sources of fine aerosols over the HTP's forest and

345   grassland areas. In the southeastern TP, strong monoterpene emissions were reported, as there

346   are a great number of alpine forest species (Wang et al., 2007); biogenic emissions were

347   identified as the main precursors of atmospheric low-weight organic acids (Liu et al., 2014).

Atmospheric
Chemistry
and Physics
Discussions

348   In the central TP, biogenic contributions to secondary organic carbon were estimated to be

349   ~75%; biogenic aerosol tracer concentrations were also higher in summer than in winter

350   (Shen et al., 2015).

351   **4 Summary and conclusions**

352   We studied aerosol mass loadings for the period 2011-2013 over the highland region of the

353   HTP on both local and regional scales, through integrating multi-station measurements with

354   satellite and ground-based remoting sensing. We found that mass concentrations of these

355   surface atmospheric aerosols were relatively low and varied with land cover, with the general

356   tendency of Ngari and QOMS (barren sites) > Nam Co (grassland site) > SET (forest site).

357    $PM_{2.5}$ concentrations at these sites were 18.2±8.9, 14.5±7.4, 11.9±4.9 and 11.7±4.7 μg m^{-3},

358   respectively. Correspondingly, their fractions (to TSP) were 27.4±6.65%, 22.3±10.9%,

359   37.3±11.1% and 54.4±6.72%. Bimodal mass distributions of size-segregated particles were

360   found at all sites, with a relatively small peak in accumulation mode and a more marked peak

361   in coarse mode. Diurnal variations in fine aerosol masses generally displayed a bi-peak

362   pattern at the QOMS, Nam Co and SET stations, and a single-peak pattern at the Ngari station,

363   controlled by the effects of local geomorphology, mountain-valley breeze circulations and

364   aerosol emissions. Minerals matter content in $PM_{2.1}$ samples was 26% at the Ngari station and

365   29% at QOMS, or ~2-3 times that of reported results at human-influenced sites. Furthermore,

366   our observations confirmed that land surface and boundary layer settings create a dynamic for

367   these fine particles to be lifted from the barren land surface into the atmosphere.

368   Combining surface aerosol and atmospheric-column aerosol optical property data, we

Atmospheric Chemistry and Physics Discussions

Open Access

EGU

369 found that TSP masses and MISR-AOD values generally decreased as land cover varied from

370 barren to forest, inversely to $PM_{2.5}$ ratios. The seasonality of aerosol mass parameters was

371 land-cover dependent. Over forest and grassland areas, TSP mass, $PM_{2.5}$ mass, MISR-AOD

372 and fine-mode AOD values were higher in spring and summer and relatively lower in autumn

373 and winter. Such spatial and seasonal variations were possibly associated with regional

374 biogenic emissions and related aerosol products. At QOMS, there were inconsistent seasonal

375 variations between surface TSP mass ($PM_{2.5}$ mass) and atmospheric column AOD (fine-mode

376 AOD).

377 This study provides new insights on understanding the mass properties of HTP atmospheric

378 aerosols. HTP aerosol masses (especially their regional characteristics and fine particle

379 emissions) need to be treated sensitively in relation to assessments of their climatic effect and

380 potential role as cloud condensation nuclei and ice nuclei.

Acknowledgements

References

389 Babu, S. S., Chaubey, J. P., Krishna Moorthy, K., Gogoi, M. M., Kompalli, S. K., Sreekanth, V., Bagare,

Atmospheric
Chemistry
and Physics
Discussions

Open Access

EGU

390   S. P., Bhatt, B. C., Gaur, V. K., Prabhu, T. P., and Singh, N. S.: High altitude (~4520 m amsl)
391   measurements of black carbon aerosols over western trans-Himalayas: Seasonal heterogeneity and
392   source apportionment, J. Geophys. Res., 116, D24201, doi: 10.1029/2011jd016722, 2011.

393 Broxton, P. D., Zeng, X., Sulla-Menashe, D., and Troch, P. A.: A Global Land Cover Climatology
394   Using MODIS Data, J. Appl. Meteorol. Climatol., 53, 1593-1605, 2014.

395 Cong, Z., Kang, S., Kawamura, K., Liu, B., Wan, X., Wang, Z., Gao, S., and Fu, P.: Carbonaceous
396   aerosols on the south edge of the Tibetan Plateau: concentrations, seasonality and sources, Atmos.
397   Chem. Phys., 15, 1573-1584, 2015.

398 Cong, Z. Y., Kang, S. C., Liu, X. D., and Wang, G. F.: Elemental composition of aerosol in the Nam Co
399   region, Tibetan Plateau, during summer monsoon season, Atmos. Environ., 41, 1180-1187, 2007.

400 Decesari, S., Facchini, M. C., Carbone, C., Giulianelli, L., Rinaldi, M., Finessi, E., Fuzzi, S., Marinoni,
401   A., Cristofanelli, P., Duchi, R., Bonasoni, P., Vuillermoz, E., Cozic, J., Jaffrezo, J. L., and Laj, P.:
402   Chemical composition of PM10 and PM1 at the high-altitude Himalayan station Nepal Climate
403   Observatory-Pyramid (NCO-P) (5079 m a.s.l.), Atmos. Chem. Phys., 10, 4583-4596, 2010.

404 Huang, J., Minnis, P., Yi, Y., Tang, Q., Wang, X., Hu, Y., Liu, Z., Ayers, K., Trepte, C., and Winker, D.:
405   Summer dust aerosols detected from CALIPSO over the Tibetan Plateau, Geophys. Res. Lett., 34,
406   doi: 10.1029/2007GL029938, 2007.

407 Kang, S., Chen, P., Li, C., Liu, B., and Cong, Z.: Atmospheric aerosol elements over the inland Tibetan
408   Plateau: concentration, seasonality, and transport, Aerosol Air Qual Res, 16, 789-800, 2016.

409 Kaufman, Y. J., Smirnov, A., Holben, B. N., and Dubovik, O.: Baseline maritime aerosol: Methodology
410   to Derive the optical thickness and scattering properties, Geophys. Res. Lett., 28, 3251-3254, 2001.

411 Lüthi, Z. L., Škerlak, B., Kim, S. W., Lauer, A., Mues, A., Rupakheti, M., and Kang, S.: Atmospheric
412   brown clouds reach the Tibetan Plateau by crossing the Himalayas, Atmos. Chem. Phys., 15,
413   6007-6021, 2015.

414 Lau, K., Kim, M., and Kim, K.: Asian summer monsoon anomalies induced by aerosol direct forcing:
415   the role of the Tibetan Plateau, Clim. Dynam., 26, 855-864, 2006.

416 Lawrence, M. G.: Atmospheric science: Asia under a high-level brown cloud, Nature Geosci., 4,
417   352-353, 2011.

418 Lin, W., Zhu, T., Song, Y., Zou, H., Tang, M., Tang, X., and Hu, J.: Photolysis of surface O_3 and
419   production potential of OH radicals in the atmosphere over the Tibetan Plateau, J. Geophys. Res.,
420   113, D02309, doi: 10.1029/2007jd008831, 2008.

421 Liu, B., Kang, S., Sun, J., Zhang, Y., Xu, R., Wang, Y., Liu, Y., and Cong, Z.: Wet precipitation
422   chemistry at a high-altitude site (3,326 m a.s.l.) in the southeastern Tibetan Plateau, Environ. Sci.
423   Pollut. Res., 20, 5013-5027, 2013.

424 Liu, B., Kang, S., Sun, J., Wan, X., Wang, Y., Gao, S., and Cong, Z.: Low-molecular-weight organic
425   acids in the Tibetan Plateau: Results from one-year of precipitation samples at the SET station,
426   Atmos. Environ., 86, 68-73, 2014.

427 Liu, Y. W., Xu, R., Wang, Y. S., Pan, Y. P., and Piao, S. L.: Wet deposition of atmospheric inorganic
428   nitrogen at five remote sites in the Tibetan Plateau, Atmos. Chem. Phys., 15, 11683-11700, 2015.

429 Liu, Z., Liu, D., Huang, J., Vaughan, M., Uno, I., Sugimoto, N., Kittaka, C., Trepte, C., Wang, Z.,
430   Hostetler, C., and Winker, D.: Airborne dust distributions over the Tibetan Plateau and surrounding
431   areas derived from the first year of CALIPSO lidar observations, Atmos. Chem. Phys., 8, 5045-5060,
432   2008.

433 Maenhaut, W., Raes, N., Chi, X., Cafmeyer, J., Wang, W., and Salma, I.: Chemical composition and

Atmospheric
Chemistry
and Physics
Discussions

434   mass closure for fine and coarse aerosols at a kerbside in Budapest, Hungary, in spring 2002, X-Ray
435   Spectrom., 34, 290-296, 2005.

436   Mbourou, G. N. T., Bertrand, J. J., and Nicholson, S. E.: The diurnal and deasonal dycles of wind-borne
437   dust over Africa North of the equator, J. Clim. Appl. Meteor., 36, 868-882, 1997.

438   Ming, J., Cachier, H., Xiao, C., Qin, D., Kang, S., Hou, S., and Xu, J.: Black carbon record based on a
439   shallow Himalayan ice core and its climatic implications, Atmos. Chem. Phys., 8, 1343-1352, 2008.

440   Panwar, T. S., Hooda, R. K., Lihavainen, H., Hyvarinen, A. P., Sharma, V. P., and Viisanen, Y.:
441   Atmospheric aerosols at a regional background Himalayan site-Mukteshwar, India, Environ. Monit.
442   Assess., 185, 4753-4764, 2013.

443   Patashnick, H., and Rupprecht, E. G.: Continuous PM-10 measurements using the Tapered Element
444   Oscillating Microbalance, J. Air Waste Manage., 41, 1079-1083, 1991.

445   Qu, B., Ming, J., Kang, S. C., Zhang, G. S., Li, Y. W., Li, C. D., Zhao, S. Y., Ji, Z. M., and Cao, J. J.:
446   The decreasing albedo of the Zhadang glacier on western Nyainqentanglha and the role of
447   light-absorbing impurities, Atmos. Chem. Phys., 14, 11117-11128, 2014.

448   Ramanathan, V., Crutzen, P. J., Lelieveld, J., Mitra, A. P., Althausen, D., Anderson, J., Andreae, M. O.,
449   Cantrell, W., Cass, G. R., Chung, C. E., Clarke, A. D., Coakley, J. A., Collins, W. D., Conant, W. C.,
450   Dulac, F., Heintzenberg, J., Heymsfield, A. J., Holben, B., Howell, S., Hudson, J., Jayaraman, A.,
451   Kiehl, J. T., Krishnamurti, T. N., Lubin, D., McFarquhar, G., Novakov, T., Ogren, J. A., Podgorny, I.
452   A., Prather, K., Priestley, K., Prospero, J. M., Quinn, P. K., Rajeev, K., Rasch, P., Rupert, S.,
453   Sadourny, R., Satheesh, S. K., Shaw, G. E., Sheridan, P., and Valero, F. P. J.: Indian Ocean
454   Experiment: An integrated analysis of the climate forcing and effects of the great Indo-Asian haze, J.
455   Geophys. Res., 106, 28371-28398, 2001.

456   Ramanathan, V., Chung, C., Kim, D., Bettge, T., Buja, L., Kiehl, J. T., Washington, W. M., Fu, Q.,
457   Sikka, D. R., and Wild, M.: Atmospheric brown clouds: Impacts on South Asian climate and
458   hydrological cycle, Proc. Natl. Acad. Sci. U.S.A., 102, 5326-5333, 2005.

459   Shen, R. Q., Ding, X., He, Q. F., Cong, Z. Y., Yu, Q. Q., and Wang, X. M.: Seasonal variation of
460   secondary organic aerosol tracers in Central Tibetan Plateau, Atmos. Chem. Phys., 15, 8781-8793,
461   2015.

462   Sheng, J., Wang, X., Gong, P., Joswiak, D. R., Tian, L., Yao, T., and Jones, K. C.: Monsoon-driven
463   transport of organochlorine pesticides and polychlorinated biphenyls to the Tibetan Plateau: three
464   year atmospheric monitoring study, Environ. Sci. Technol., 47, 3199-3208, 2013.

465   Stout, J. E.: Diurnal patterns of blowing sand, Earth Surf Proc Land, 35, 314-318, 2010.

466   Vernier, J. P., Thomason, L. W., and Kar, J.: CALIPSO detection of an Asian tropopause aerosol layer,
467   Geophys. Res. Lett., 38, doi: L07804, 10.1029/2010gl046614, 2011.

468   Wang, Q., Han, Z., Tijian, W., and Yoshiro, H.: An estimate of biogenic emissions of volatile organic
469   compounds during summertime in China, Environ. Sci. Pollut. Res., 14, 69-75, 2007.

470   Willeke, K., and Whitby, K. T.: Atmospheric aerosols: size distribution interpretation, J. Air Pollut.
471   Control Assoc., 25, 529-534, 1975.

472   Xia, X., Wang, P., Wang, Y., Li, Z., Xin, J., Liu, J., and Chen, H.: Aerosol optical depth over the Tibetan
473   Plateau and its relation to aerosols over the Taklimakan Desert, Geophys. Res. Lett., 35, doi:
474   10.1029/2008gl034981,2008.

475   Xia, X., Zong, X., Cong, Z., Chen, H., Kang, S., and Wang, P.: Baseline continental aerosol over the
476   central Tibetan plateau and a case study of aerosol transport from South Asia, Atmos. Environ., 45,
477   7370-7378, 2011.

Atmospheric
Chemistry
and Physics
Discussions

Open Access

478   Xin, J., Wang, Y., Pan, Y., Ji, D., Liu, Z., Wen, T., Wang, Y., Li, X., Sun, Y., Sun, J., Wang, P., Wang, G.,
479   Wang, X., Cong, Z., Song, T., Hu, B., Wang, L., Tang, G., Gao, W., Guo, Y., Miao, H., Tian, S., and
480   Wang, L.: The campaign on atmospheric aerosol research network of China: CARE-China, Bull.
481   Amer. Meteor. Soc., 96, 1137-1155, 2015.
482   Xu, B., Cao, J., Hansen, J., Yao, T., Joswia, D. R., Wang, N., Wu, G., Wang, M., Zhao, H., Yang, W.,
483   Liu, X., and He, J.: Black soot and the survival of Tibetan glaciers, Proc. Natl. Acad. Sci. U.S.A.,
484   106, 22114-22118, 2009.
485   Xu, J., Wang, Z., Yu, G., Qin, X., Ren, J., and Qin, D.: Characteristics of water soluble ionic species in
486   fine particles from a high altitude site on the northern boundary of Tibetan Plateau: Mixture of
487   mineral dust and anthropogenic aerosol, Atmos. Res., 143, 43-56, 2014.
488   Yan, N., Wu, G., Zhang, X., Zhang, C., Xu, T., and Lazhu: Variation of aerosol optical properties from
489   AERONET observation at Mt. Muztagh Ata, Eastern Pamirs, Atmos. Res., 153, 480-488, 2015.
490   Zhang, X. Y., Arimoto, R., Cao, J. J., An, Z. S., and Wang, D.: Atmospheric dust aerosol over the
491   Tibetan Plateau, J. Geophys. Res., 106, 18471-18476, 2001.
492   Zhang, Y., Sillanpää M., Li, C., Guo, J., Qu, B., and Kang, S.: River water quality across the
493   Himalayan regions: elemental concentrations in headwaters of Yarlung Tsangbo, Indus and Ganges
494   River, Environ Earth Sci, 1-13, doi: 10.1007/s12665-014-3702-y, 2014.
495   Zhao, Z., Cao, J., Shen, Z., Xu, B., Zhu, C., Chen, L. W. A., Su, X., Liu, S., Han, Y., Wang, G., and Ho,
496   K.: Aerosol particles at a high-altitude site on the Southeast Tibetan Plateau, China: Implications for
497   pollution transport from South Asia, J. Geophys. Res., 118, 11360-11375, 2013.
498

Atmospheric
Chemistry
and Physics
Discussions

499 **Table**

500 Table 1. Geographical conditions and aerosol observations at HTP background sites (Ngari, QOMS, Nam Co and SET stations).

501

Station	Location	Altitude (asl)	Description	Research content	Observation	Instrumentation
Ngari station	79°42'E 33°23'N	4,264 m	Semi-arid area, western TP	1. Online and size distribution of aerosol masses;	1. PM$_{2.5}$ (/5 min) and nine-stage aerosol mass (weekly);	1. TEOM RP1400 and nine-stage Anderson samplers;
QOMS station	86°57'E 28°21'N	4,300 m	North slope of the central Himalaya	2. Chemical composition and matter closure of size-segregated aerosols;	2. Soluble salts, heavy metals, OC and EC (biweekly);	2. IC, ICP-MS and thermal optical carbon analyzer;
Nam Co station	90°57'E 30°46'N	4,746 m	Alpine grassland, central TP	3. Aerosol optical properties	3. Aerosol optical depth and Angstrom exponent (hourly)	3. Microtops II sunphotometer at Ngari and SETS stations, *CIMEL sunphotometer at QOMS and Nam Co stations
SET station	94°44'E 29°46'N	3,326 m	Alpine forest, southeastern TP			

502

503 *The QOMS and Nam Co stations are also Aerosol Robotic Network (AERONET) sites (http://aeronet. gsfc.nasa.gov/). The abbreviations IC,

504 ICP-MS and TEOM stand for ion chromatography, inductively coupled plasma mass spectroscopy and tapered element oscillating microbalance,

505 respectively.

506

507

Atmospheric
Chemistry
and Physics
Discussions

Open Access

EGU

Table 2. Concentrations ($\mu g\ m^{-3}$) of hourly, daily and baseline $PM_{2.5}$ and differences ($\mu g\ m^{-3}$) between online and baseline $PM_{2.5}$ at four HTP stations for 2011-2013. Num and S.D. stand for number and standard deviation, respectively.

$PM_{2.5}$	Ngari station			QOMS station			Nam Co station			SET station		
	Num	Range	Mean±S.D.	Num	Range	Mean±S.D.	Num	Range	Mean±S.D.	Num	Range	Mean±S.D.
Hourly	1963	0.2-267.4	18.5±24.3	4049	0.1-99.7	13.8±12.3	11067	0.2-98.8	11.8±8.1	6871	0.1-78.5	11.7±10.0
Daily	88	7.1-77.3	18.2±8.9	236	2.6-48.1	14.5±7.4	480	3.9-43.9	11.9±4.9	351	2.8-28.7	11.7±4.7
Baseline	1594	4.9-24.4	11.2±3.2	1658	2.6-18.4	9.8±3.1	8880	3.3-28.4	9.8±3.6	4032	2.7-20.3	9.2±3.0
Online-Baseline	1477	-16.3-109.7	4.2±14.0	1431	-15.7-53.7	2.1±2.0	8590	-17.7-33.0	0.8±5.3	3554	-13.9-49.4	1.2±6.6

Atmospheric
Chemistry
and Physics
Discussions

Open Access

EGU

525 Table 3. Average mass concentrations ± standard deviations (μg m^{-3}) for

526 size-segregated particles (at various μm) and PM$_{1.1}$, PM$_{2.1}$, PM$_9$ and TSP sampled

527 from the HTP surface atmosphere during 2011-2013. Num stands for number of

528 samples.

529

Species	Ngari station	QOMS station	Nam Co station	SET station
Num	54	89	65	66
<0.43	7.7±5.1	5.8±6.0	4.1±4.3	2.6±2.6
0.43-0.65	8.8±5.8	6.6±6.2	3.7±3.4	2.4±2.1
0.65-1.1	7.5±3.6	6.5±5.0	3.6±4.5	2.6±2.2
1.1-2.1	7.0±3.8	7.6±6.8	3.2±3.1	2.3±2.0
2.1-3.3	8.1±5.5	7.1±5.5	3.3±3.5	2.3±2.1
3.3-4.7	7.2±3.6	8.3±11.1	3.4±3.8	2.5±2.0
4.7-5.8	7.2±3.4	8.3±10.5	3.4±4.0	2.4±2.2
5.8-9	7.8±7.1	7.7±5.9	3.7±4.9	2.0±1.6
>9	5.6±8.2	7.8±6.6	3.5±4.1	2.3±3.5
PM$_{1.1}$	24±14.5	18.9±17.3	11.3±12.2	7.7±6.8
PM$_{2.1}$	30.6±14.2	26.3±20.6	14.5±12.9	10.0±8.2
PM$_9$	60.9±27.5	57.5±45.4	28.4±25.9	19.2±15.0
TSP	66.4±29.6	65.1±50.9	31.9±29.0	21.5±18.0

530
531
532
533
534
535
536
537
538
539
540
541
542
543
544
545
546
547
548

Atmospheric
Chemistry
and Physics
Discussions

549　**Figures**

550
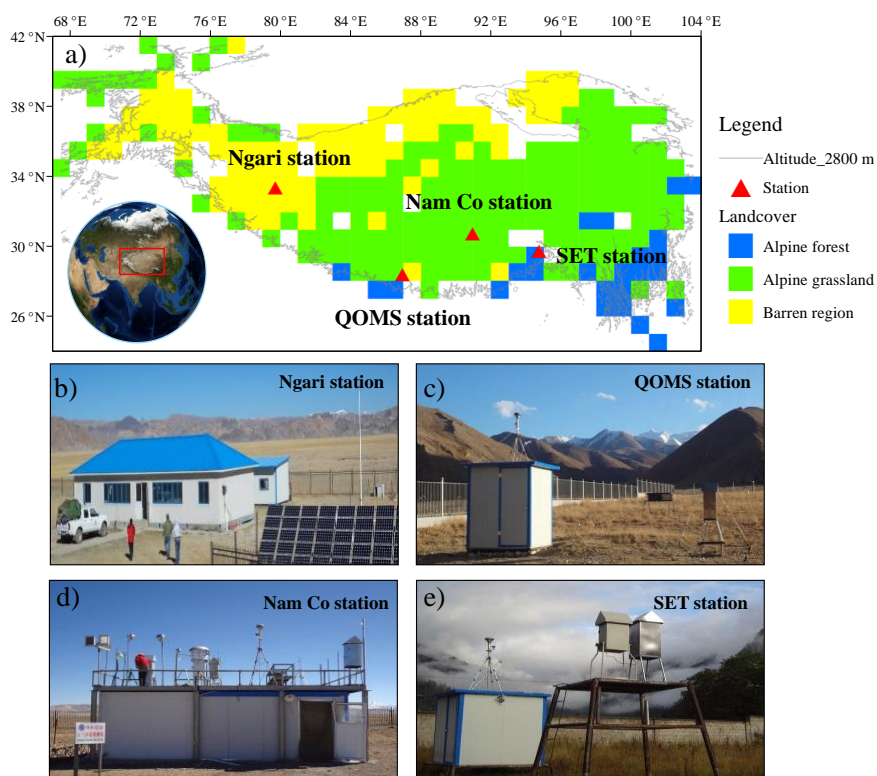
551

552　Fig. 1. The main landscapes (1×1 degree pixel resolution) (a) and the aerosol

553　observation sites in the HTP (b, c, d, e). The highland HTP region is taken as land

554　above 2800 m asl but the thresholds are 1500 m asl for areas 92-97 °E and 26-34 °N,

555　and 2000 m asl for areas 98-104 °E and 24-34 °E, accounting for the regional

556　deviations caused by the extremely steep topography. The classification of landscapes,

557　according to MODIS land cover classification (Broxton et al., 2014), suggests

558　different land covers at these stations (here the forest areas comprise evergreen, mixed,

559　and deciduous forests).

560

561

Atmospheric
Chemistry
and Physics
Discussions

562

563
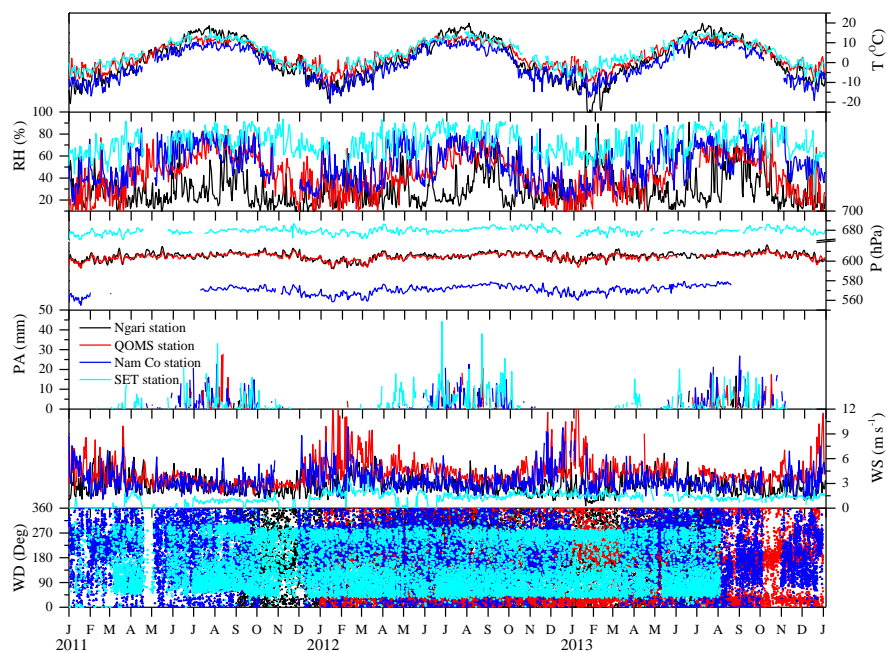
Fig. 2. Time series for hourly air temperature (T), relative humidity (RH), pressure (P),

precipitation amount (PA), wind speed (WS) and wind direction (WD) in the HTP

during 2011-2013, at the Ngari station (black), the QOMS station (red), the Nam Co

station (blue), and the SETS station (cyan), respectively.

568
569
570
571
572
573
574
575
576
577
578
579
580
581
582
583

Atmospheric
Chemistry
and Physics
Discussions

Open Access

EGU

584
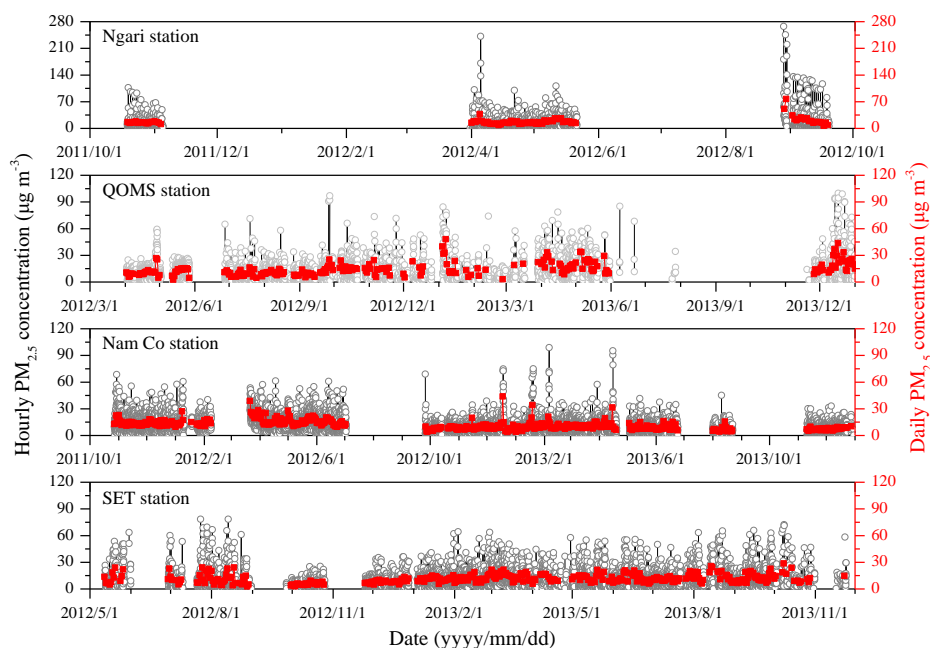
585

586　Fig. 3. Hourly and daily mean concentrations (μg m^{-3}) of PM$_{2.5}$ at the Ngari station

587　(Oct. 2011-Oct. 2012), the QOMS station (Mar. 2012-Dec. 2013), the Nam Co station

588　(Oct. 2011-Dec. 2013), and the SET station (May. 2011-Dec. 2013) in the HTP.

589　Periods with no data were due to power supply problems or equipment breakdown. A

590　daily mean was calculated only when at least eight hourly means were available

591　during that day.

592

593

594

595

596

597

598

599

600

601

602

603

604

Atmospheric
Chemistry
and Physics
Discussions
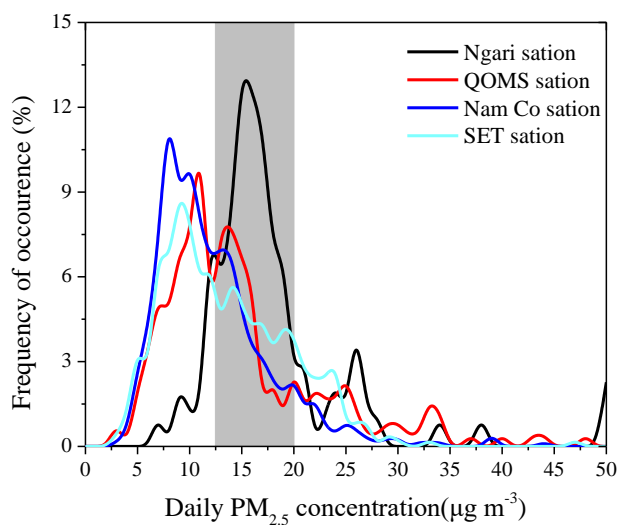
605

606 Fig. 4. Frequency distributions of daily $PM_{2.5}$ concentrations over the HTP observed

607 during the 2011-2013 period. High-concentration peaks around the range of 12.5-20

608 $\mu g\ m^{-3}$ occurred in the frequency curves of the Ngari and QOMS stations, as indicated

609 by the grey shading. The maximum $PM_{2.5}$ bin concentration was set to 50 $\mu g\ m^{-3}$,

610 although a small fraction existed at higher concentrations.

611
612
613
614
615
616
617
618
619
620
621
622
623
624
625
626
627
628
629
630

Atmospheric
Chemistry
and Physics
Discussions

631
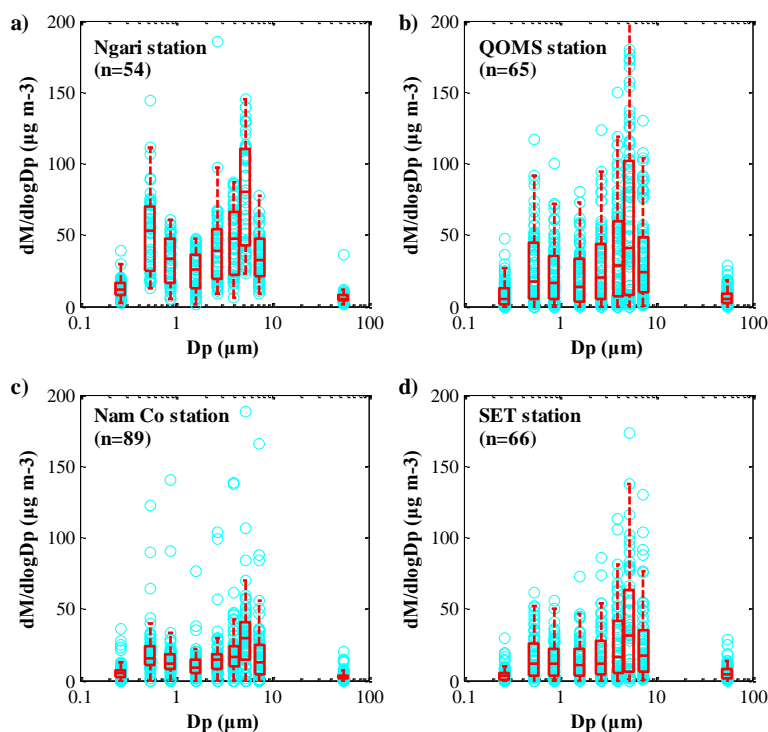
632

633 Fig. 5. Size distributions of mass aerosol particles in the background surface

634 atmosphere of the HTP (a: Ngari station, b: QOMS station, c: Nam Co station, d: SET

635 station) as observed over the 2011-2013 period. Boxes show the percentile values (25,

636 50, 75) and whisker plots show maximum and minimum of non-outliers numbers, and

637 the small blue circles behind the boxes are the distribution points.

638
639
640
641
642
643
644
645
646
647
648
649

Atmospheric
Chemistry
and Physics
Discussions

Open Access

EGU
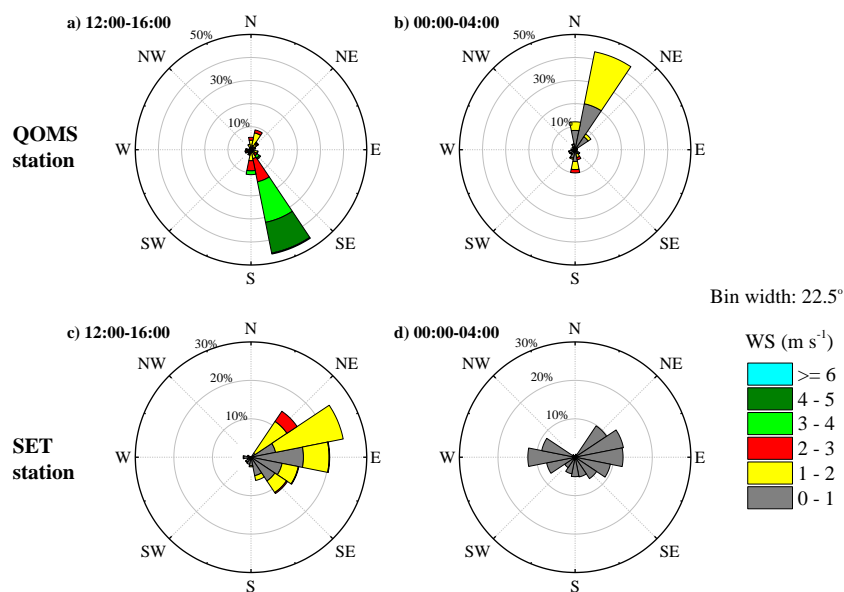
650

651 Fig. 6. Wind rose plots for afternoon (12:00-16:00 LT) and nighttime (00:00-04:00

652 LT) in July and August at the QOMS station (a, b) and the SET station (c, d). An

653 hourly horizontal wind direction (WD) was used, with its radii values expressed as

654 percentages for wind blowing from particular directions.

655
656
657
658
659
660
661
662
663
664
665
666

Atmospheric
Chemistry
and Physics
Discussions

667
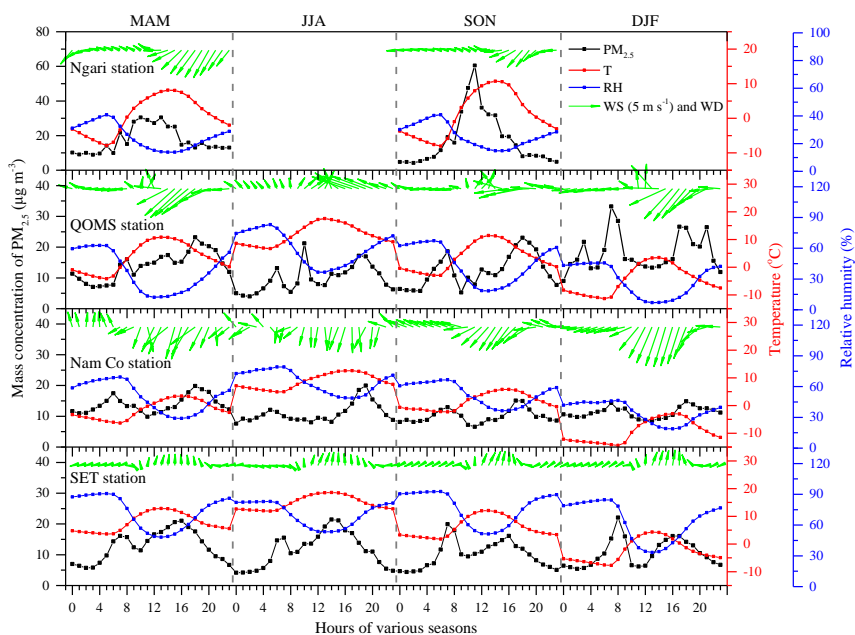
668

669   Fig. 7. Seasonal diurnal variations in PM$_{2.5}$ concentrations, air T and RH over the

670   2011-2013 period at four background HTP sites (the Ngari station, the QOMS station,

671   the Nam Co station and the SET station). The local time (LT) was used at each site,

672   according to longitudinal position.

673
674
675
676
677
678
679
680
681
682
683
684
685
686
687
688
689

Atmospheric
Chemistry
and Physics
Discussions

Open Access

690
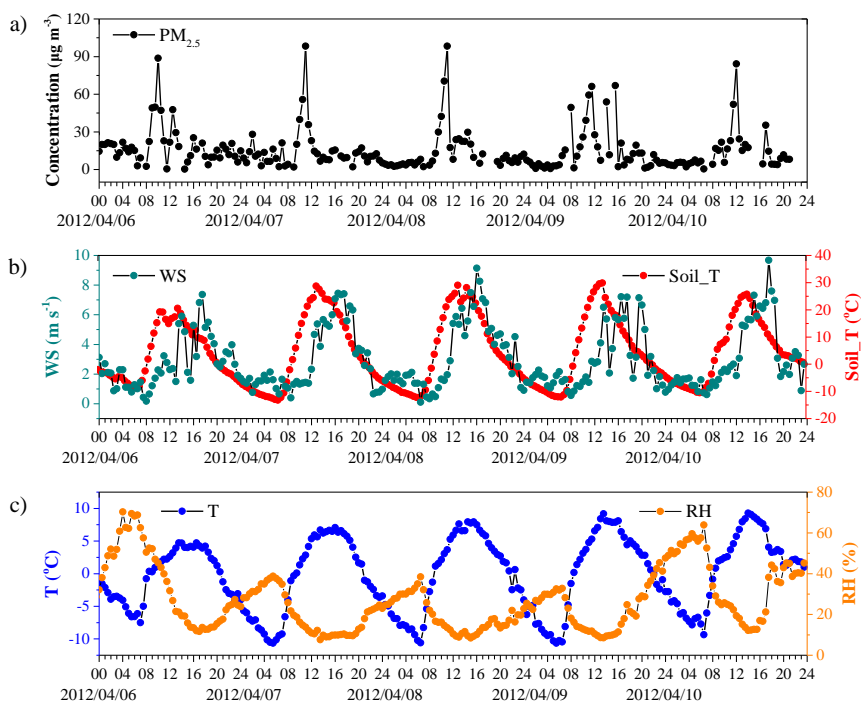
691

692   Fig. 8. Diurnal variations in PM$_{2.5}$ masses and related environmental factors for April

693   6th-10th 2012 at the Ngari station (located in a typical barren and arid area of inland

694   Asia). SR is downward shortwave radiation and soil T is the surface soil temperature

695   at 0 cm. The local time (LT) and a 30 min mean were used.

696
697
698
699
700
701
702
703
704
705
706

Atmospheric
Chemistry
and Physics
Discussions

Open Access
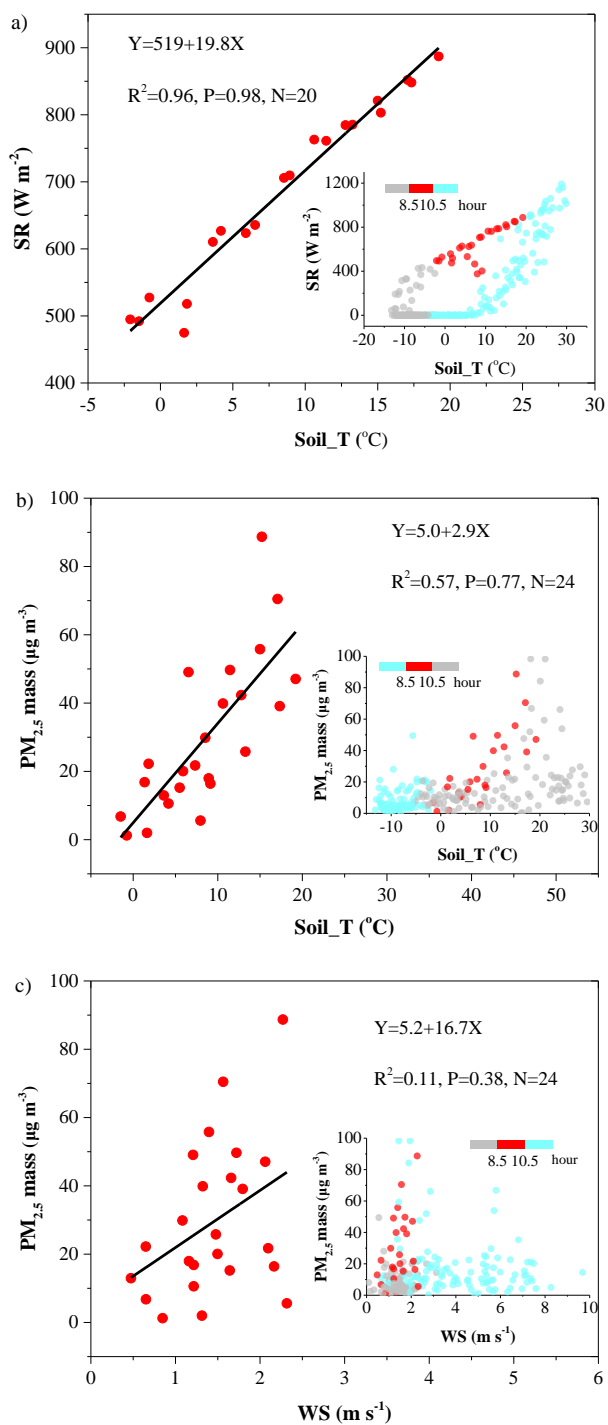
707

708   Fig. 9. Correlations between SR and soil T (a), soil T and PM$_{2.5}$ mass (b), and WS and

709   PM$_{2.5}$ mass (c) during the morning (8:30-10:30 LT) at the Ngari station, for April

710   6th-10th 2012. The smaller inserts show all recorded points within the measured

711   timeframe. Note that the fit line of Figure 9a is for April 6th-9th 2012, because there

712   was a rainfall event (~8:00-11:00 LT) on April 10th 2012, as indicated in Figure 8.

713   However, even if the dataset for April 10th 2012 is included, the fit line remains more

714   or less consistent, with R^2=0.61 and P=0.79. The local time (LT) and a 30 min mean

715   were used.

716

717

718
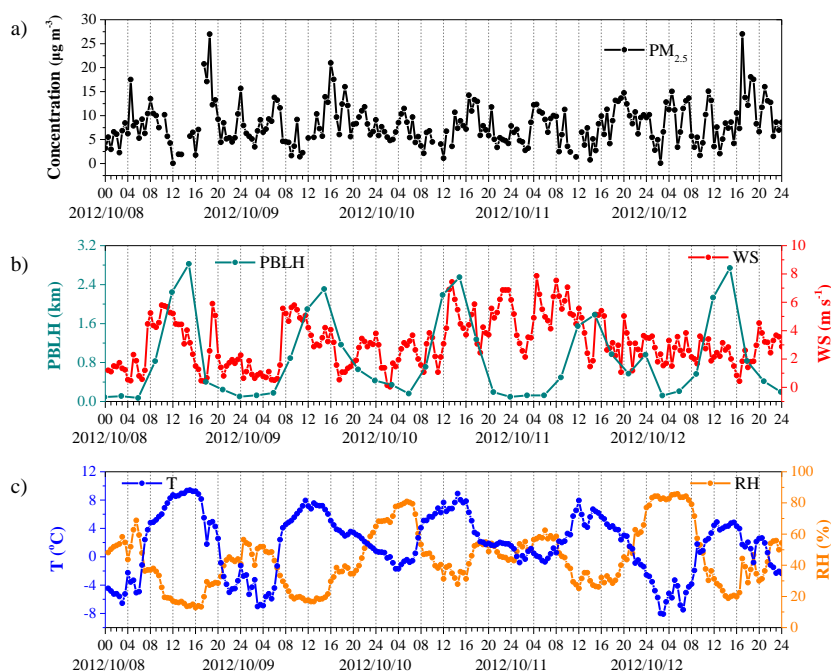
719

720   Fig. 10. Diurnal variations in PM$_{2.5}$ concentrations and related environmental factors

721   for October 8th-12th 2012 at the Nam Co station. 30 min mean datasets were used,

722   based on local time (LT).

723

724

34

725

a) **TSP concentration and MISR AOD (at 550 nm)**

b) **PM$_{2.5}$ ratio (to TSP) and Fine-mode fraction (at 550 nm)**
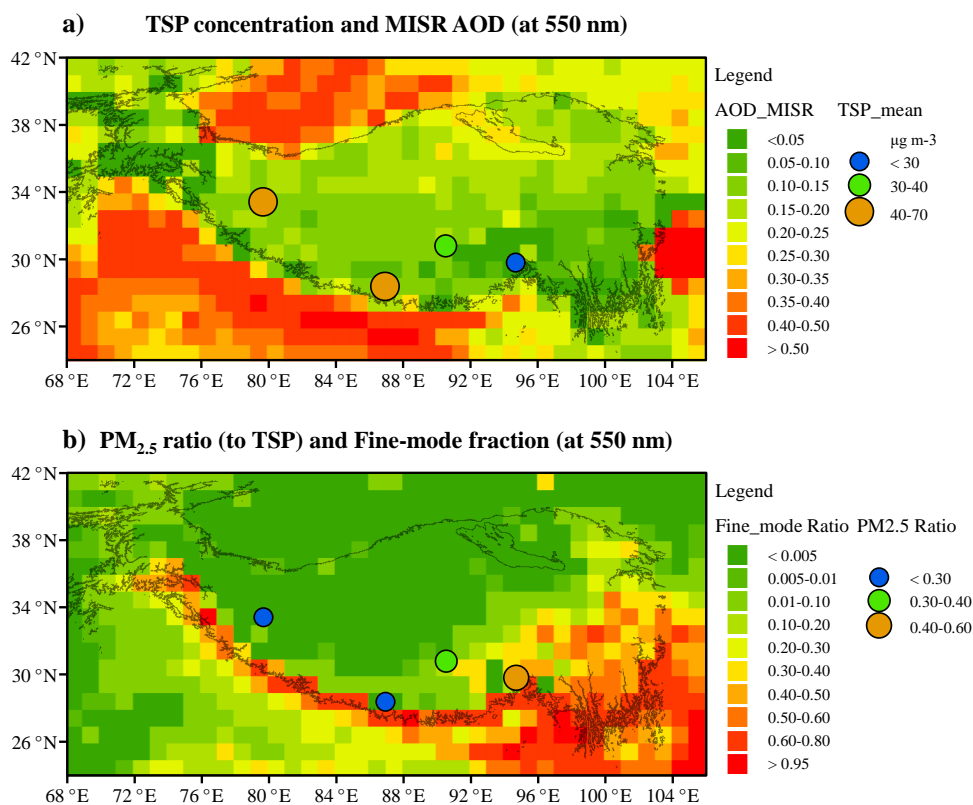
726

727   Fig. 11. Spatial patterns in AOD and TSP mass (a) and aerosol fine-mode fraction and

728   the ratio of PM$_{2.5}$ to TSP (b) over the HTP. Figure 11a shows mean MISR AOD (at

729   550 nm) for 2011-2013 as derived from monthly Level 3 datasets. Figure 11b shows a

730   time-average map of the MODIS fine-mode fraction (at 550 nm) for 2011-2013,

731   according to monthly Terra (version 5.1) Level 3 values. Ground-based observations

732   are average values sampled in 2011-2013.

733

734

735

736

737

738

739

740
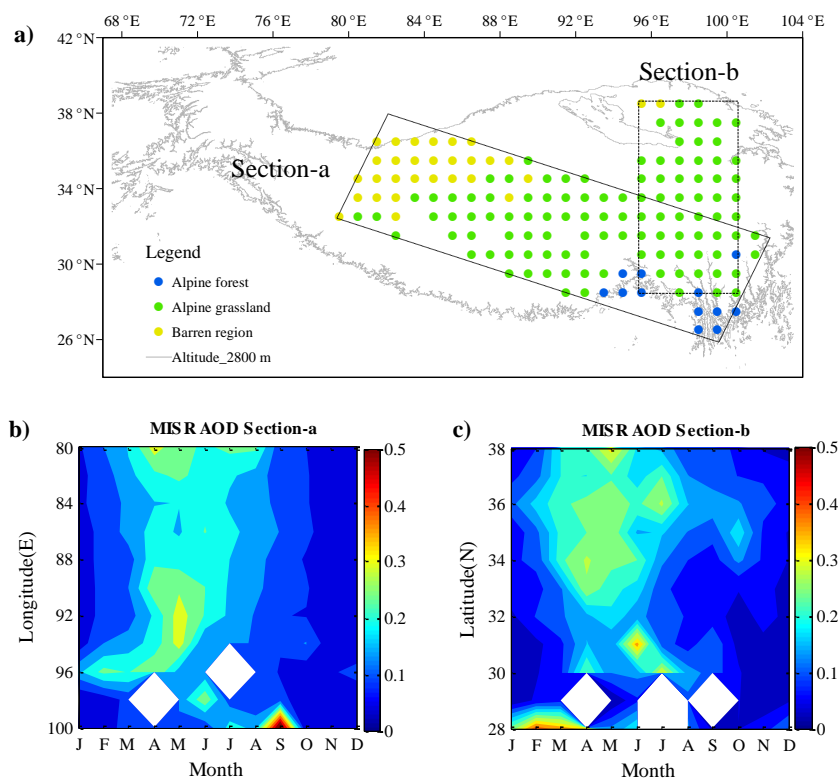
Fig. 12. Mean MISR AOD (at 550 nm) for two cross-sections during various months in the 2011-2013 period. Missing datasets are plotted in white. The longitudinal Section A is from the southeast (100 °E, 25.5 °N-102 °E, 31.5 °N) to the northwest (79.5 °E, 32.5 °N-81.5 °E, 38.5 °N); the latitudinal Section B is from the south (95 °E, 28 °N-101 °E, 28 °N) to the north (95 °E, 39 °N-101 °E, 39 °N). J-D stands for the months of January-December.

747

748

749

750
751
752
753
754

Atmospheric
Chemistry
and Physics
Discussions
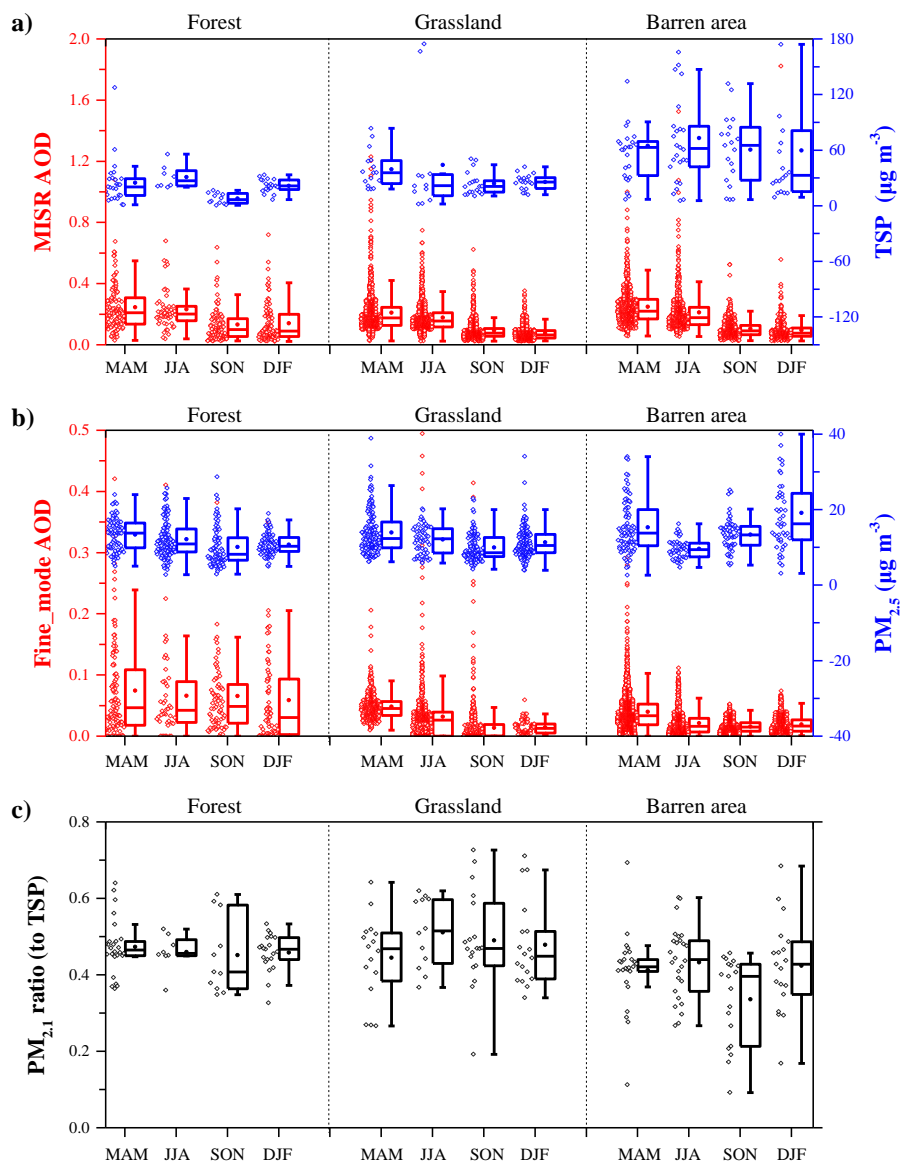
Fig. 13. Seasonal characteristics of landscape-classified aerosol masses in the HTP, based on *in situ* observations and remote sensing datasets. The MISR-AOD (at 550 nm) values in Figure 13a are monthly Level 3 datasets for the 2011-2013 period over the HTP, and were classified based on landscape. The fine-mode AOD (at 500 nm)

760 data for barren and grassland sites were obtained from AERONET results at the

761 QOMS station and the Nam Co station, respectively (Fig. 13b). Fine-mode AOD (at

762 550 nm) data for the forest area in Figure 13b were estimated, based on monthly

763 MODIS Terra (version 5.1) Level 3 results, using the formula fine-mode AOD (at 550

764 nm) = AOD (at 550 nm) * fine-mode fraction (at 550 nm). Site land cover

765 classifications are: alpine forest at the SETS station; alpine grassland at the Nam Co

766 station; and barren land cover at the QOMS station. Boxes show the percentile values

767 (25, 50, 75) and whisker plots show maximum and minimum of non-outliers numbers,

768 and the small point within each box is the mean value. The abbreviations are March–

769 May: MAM; June–August: JJA; September–November: SON; and December–

770 February: DJF.

771

772

773

774

775